



Magnetic sporopollenin supported magnesium nanoparticles for removal of tetracycline as an emerging contaminant from water

Jari S. Algethami^{1,2} · Krishna Kumar Yadav^{3,4,5} · Amel Gacem⁶ · Ismat H. Ali⁷ · Shahabaldin Rezanian⁸ · Munirah Sulaiman Othman Alhar⁹ · Amine Mezni¹⁰ · Byong-Hun Jeon¹¹ · Sumate Chairapat⁴

Received: 22 January 2023 / Accepted: 1 June 2023 / Published online: 9 June 2023
© The Author(s), under exclusive licence to Springer-Verlag GmbH Germany, part of Springer Nature 2023

Abstract

Since the release of antibiotics as emerging contaminants into the environmental water can cause severe difficulties for human health, their removal from the water is necessary. In this regard, a novel environmentally friendly adsorbent was developed based on green sporopollenin, which was magnetized and modified with magnesium oxide nanoparticles to produce MSP@MgO nanocomposite. The newly developed adsorbent was applied to remove tetracycline antibiotic (TC) from aqueous media. The surface morphology of the MSP@MgO nanocomposite was characterized using FTIR, XRD, EDX, and SEM techniques. The effective parameters of the removal process were studied, and it was confirmed that the chemical structure of TC was highly affected by changes in pH solution due to different pKa; therefore, the results showed that pH 5 was the optimum. Also, the maximum sorption capacity of MSP@MgO for TC for adsorption was obtained at 109.89 mg.g⁻¹. In addition, the adsorption models were investigated, and the process was fitted with the Langmuir model. Thermodynamic parameters showed that the process was spontaneous ($\Delta G < 0$), endothermic ($\Delta H > 0$) and the adsorption mechanism was following the physisorption mechanism at room temperature.

Keywords Sporopollenin · Tetracycline · Magnesium oxide nanoparticles

Responsible Editor: Tito Roberto Cadaval Jr

✉ Krishna Kumar Yadav
envirokrishna@gmail.com

✉ Sumate Chairapat
sumate.ch@psu.ac.th

¹ Department of Chemistry, College of Science and Arts, Najran University, P.O. Box, 1988, Najran 11001, Saudi Arabia

² Promising Centre for Sensors and Electronic Devices (PCSED), Najran University, Najran 11001, Saudi Arabia

³ Faculty of Science and Technology, Madhyanchal Professional University, Ratibad, Bhopal 462044, India

⁴ Department of Civil and Environmental Engineering, Faculty of Engineering, PSU Energy Systems Research Institute, Prince of Songkla University, Hat Yai, Songkhla 90110, Thailand

⁵ Environmental and Atmospheric Sciences Research Group, Scientific Research Center, Al-Ayen University, Thi-Qar, Nasiriyah 64001, Iraq

⁶ Department of Physics, Faculty of Sciences, University 20 Aout 1955, 21000 Skikda, Algeria

⁷ Department of Chemistry, College of Science, King Khalid University, P. O. Box 9004, Abha 61413, Saudi Arabia

⁸ Department of Environment and Energy, Sejong University, Seoul 05006, South Korea

⁹ Department of Chemistry, College of Science, University of Ha'il, Ha'il 81451, Saudi Arabia

¹⁰ Department of Chemistry, College of Science, Taif University, P.O. Box 11099, Taif 21944, Saudi Arabia

¹¹ Department of Earth Resources & Environmental Engineering, Hanyang University, 222-Wangsimni-ro, Seongdong-gu, Seoul 04763, Republic of Korea

Introduction

Antibiotics as emerging contaminants have recently been taken into account worldwide due to their diverse effects on human and environmental health in long-term exposure (Koch et al. 2021) (Chaturvedi et al. 2021; Koch et al. 2021). Although antibiotics have a vital role in healthcare by contributing to the control of diseases and the treatment of bacterial infections in humans and animals (Krasucka et al. 2021; Zainab et al. 2020). But the World Health Organization (WHO) has shown concern about the residual pharmaceutical compounds in water resources since 1997 (Maged et al. 2020). Because releases of antibiotics onto the soil and environmental water resources have substantial consequences, such as a wide variety of repercussions which can cause severe toxicity to the ecosystem and pose a negative impact on human health and ecology as well as increase the antibiotic-resistant bacteria (Du et al. 2021; Priya and Radha 2017)(Xu et al. 2021). Among antibiotics, tetracycline (TC) is the most common antibiotic across the world because of its efficient treatment in the suppression of infections. The concentration of TC is reported in the range of 0.1 to 7.8 $\mu\text{g}\cdot\text{L}^{-1}$ in wastewater (Ngigi et al. 2020) and 48–532 $\mu\text{g}\cdot\text{L}^{-1}$ in surface drains (Muriuki et al. 2020). Nations do have not restrict regulations yet and research on this issue is necessary (Shao and Wu 2020). Considering the disadvantages of antibiotics in particular TC in the environment, the elimination of this drug is essential (Liao et al. 2021; Saadati et al. 2016).

Various technologies have been used for the treatment of antibiotics reduction from the environment such as electrochemistry, ozonation, quantum dots, oxidation, membrane filtration, reverse osmosis, bioremediation, and adsorption (Alvand et al. 2019; dos Santos et al. 2021; Koch et al. 2021; Wang et al. 2019). Roughly some of these techniques are expensive and need complex equipment to scale up. Hence, among the aforementioned methods, the adsorption process is the most common approach for the removal/adsorption of antibiotics from aquatic environments (Cai et al. 2019; Krasucka et al. 2021). In recent decades, green and synthetic materials have been utilized as adsorbents for the treatment of antibiotics, such as chitosan, mesoporous silica, MOF, carbon-based materials, biopolymers, and metal oxide nanoparticles (Ahmed 2017; Du et al. 2021; Kabir et al. 2022; Li et al. 2020; Wang et al. 2019). The proposed materials provided various forces interactive with TCs such as appropriate electrostatic interactions, H-bonding, π - π and n - π electron and donor-acceptor interactions (Wang et al. 2019; Zhang et al. 2019). In this regard, green biopolymers present a good force to interact with antibiotic drugs and have the potential to be an alternative adsorbent material.

Sporopollenin as a plant-based green biopolymer has drawn the attraction of researchers as a natural and efficient adsorbent for the remediation of organic and inorganic pollutants in the environment owing to its high resilience and unique morphology (Kamboh et al. 2021; Yaacob et al. 2022). Also, the honey-comb-like structure of sporopollenin makes it an efficient host for binding with various nanoparticles and adsorbates. The backbone of sporopollenin is made of biopolymers of carbon, oxygen, and hydrogen with straight and branched aliphatic chains (Ageitos et al. 2021; Dyab et al. 2018).

Therefore, the objective of this study was to develop a novel adsorbent based on magnetic sporopollenin doped with magnesium oxide nanoparticles (MSP@MgO) for the removal of tetracycline (TC) from aquatic environments. In this regard, magnetic nanoparticles were used to boost the dispersity of hydrophobic sporopollenin in the water and ease separation by external magnetic. Moreover, embedding metallic magnesium oxide nanoparticles (MgO) provided a high surface affinity resulting in higher adsorption efficiency for the removal of antibiotics in wastewater.

In the current study, the MSP@MgO provided high adsorption capacity for TC due to the binary and multifunctional nature of nanocomposite including carbonyl, oxygen, and metal cation, which were made hydrophobic interactions, π -cation, electrostatic force interactive, and H-bonding with TC.

Experimental

Reagent and chemical

Magnesium nitrate hexahydrate, sodium hydroxide, iron (III) chloride hexahydrate, iron (II) chloride tetrahydrate, ammonia 32%, and methanol were obtained from the Merck group (Darmstadt, Germany). Lycopodium clavatum (sporopollenin) with a particle size of ~ 25 m was bought from Sigma Aldrich (St. Louis, USA). Tetracycline 99% analytical grade was purchased from Solar Biochemical Company (Beijing, China).

Instruments

The morphology of MgO nanoparticles was evaluated with a FESEM instrument (TESCAN MIRA3, Prague, Czech), and the surface structure of the sporopollenin and MSP@MgO was recorded with SEM (Zeiss Supra 35VP, MN, USA). The elemental composition of the nanocomposite was analyzed with an EDX accessory equipped with FESEM. The high resolution of the nanostructure's surface was monitored with TEM (JEOL, Tokyo, Japan). The

functional groups were recorded with FTIR in transmission mode in the wavenumber range of 400–4000 cm^{-1} (Thermo Electron, Tokyo, Japan). The crystalline nature of the nanoparticles and MSP@MgO were recorded with XRD at 40 kV $\text{CuK}\alpha$ (Bruker, Karlsruhe, Germany). The magnetic properties of nanoparticles were analyzed with a vibrating sample magnetizer (LakeShore 7400, Westerville, OH) with an applied field of 16.7 Oe and a magnet air gap of 1.5 inches.

Synthesis adsorbent

Synthesis of magnesium oxide nanoparticles

Initially (Fig. 1), 5 g of magnesium nitrate hexahydrate was dissolved in 50 mL of distilled water (DW) and sonicated for 30 h, then sodium hydroxide (2 M) was added slowly. Next, this solution was stirred for 5 h. Ultimately, the magnesium hydroxide was formed, and after washing with excess distilled water, it dried at 80 °C overnight. Finally, to achieve desired nanoparticles, they were kept in the furnace at 300 °C for 3 h.

Synthesis magnetic sporopollenin

Magnetic sporopollenin (MSP) was prepared according to the previous methods (Kamboh et al. 2021). At first, 1.9 g $\text{FeCl}_3 \cdot 6\text{H}_2\text{O}$, 2.8 g $\text{FeCl}_2 \cdot 4\text{H}_2\text{O}$, 10 mL ethanol, and 10 mL HCl (37%) were mixed in the 40 mL DW and stirred until all salt was solved completely. After achieving a homogenous solution, 1 g sporopollenin was added to the solution and stirred for 2 h. In the next step, the solution was filtered; then transferred to 30 mL prepared ammonia solution (1 M) and stirred vigorously for 2 h. Ammonia solution participates in the Fe^{3+} and Fe^{2+} ions as Fe_2O_3 iron oxide nanoparticles over sporopollenin. Eventually, the black precipitation (Fe_2O_3), which was magnetic sporopollenin, was achieved and separated from the solution by applying an external

magnet and washed with excess DW and ethanol, and oven dried at 60 °C for 24 h.

Synthesis MSP@MgO nanocomposite

In this regard (Fig. 1), 1 g of MSP was dispersed in 100 mL of methanol 20% and sonicated for 30 min. Then, different amounts of freshly prepared MgO nanoparticles (0.1, 0.3, 0.5, and 1 g) were added to the mixture and sonicated for an extra 1 h. Thereafter, the mixture was stirred for 5 h and separated with the assistance of an external magnet. Finally, the MSP@MgO product was washed with excess DW and methanol and dried at 60 °C for 24 h.

Adsorption procedure

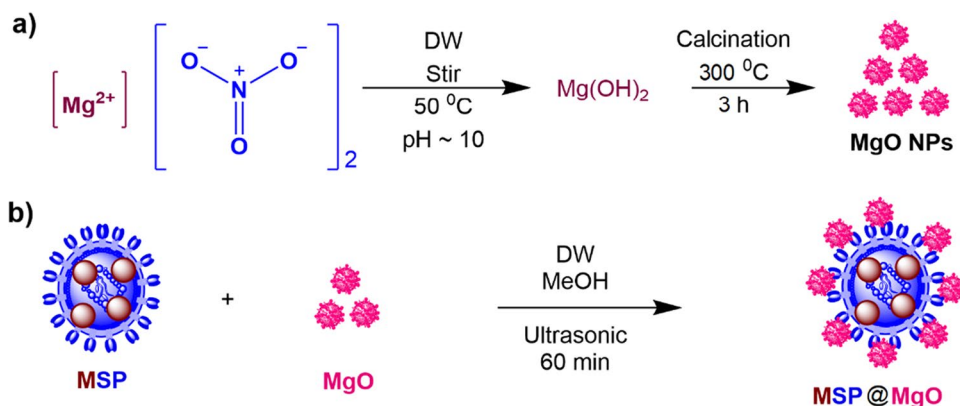
The removal or adsorption of tetracycline from water samples was studied with the batch-wise method. The appropriate amount of adsorbent was added to the 40 mL water samples including tetracycline with a proper concentration of 5–200 $\text{mg} \cdot \text{L}^{-1}$. The solution's pH was adjusted at 2–10 for different batches. Then, MSP@MgO as adsorbent (5–250 mg) was added into the aqueous solution followed by shaking for different interval times (10–250 min) at 300 rpm. After each batch adsorption process, the magnetic adsorbent was separated from aqueous media with the assistance of an external magnet. Finally, the residual concentration was recorded with ultra-violet visible spectrophotometry (UV-Visible) at 358 nm. The removal efficiency ($R\%$) is calculated with Eq. 1 and adsorption capacity (q_e , $\text{mg} \cdot \text{g}^{-1}$) was calculated based on Eq. 2.

$$R\% = ((C_0 - C_e)/C_0) \times 100 \quad (1)$$

$$q_e = \left(\frac{V}{m}\right) \times (C_0 - C_e) \quad (2)$$

where C_0 ($\text{mg} \cdot \text{L}^{-1}$) is the initial concentration of tetracycline before adsorption, C_e ($\text{mg} \cdot \text{L}^{-1}$) residual concentration

Fig. 1 The synthesis of MgO nanoparticles and MSP@MgO nanocomposites



of tetracycline after the adsorption process, V (mL) sample volume, m (mg) mass of adsorbent, and q_e ($\text{mg}\cdot\text{g}^{-1}$) equilibrium adsorption capacity.

Results and discussion

Characterization of adsorbent

Microscopy techniques

The verification of the surface morphology of sporopollenin, MgO nanoparticles, and MSP@MgO was studied using scanning electron microscopy. Figure 2a shows the surface structure of sporopollenin which had different irregular layers and crossed soft walls. This microstructure was an appropriate host to support the nanoparticles. Figure 2b shows the microstructure of MgO nanoparticles with irregular shape and size which was due to low calcination temperature. Figure 2c displays the surface morphology of MSP@MgO nanocomposite that had large gaps between the walls related to the internal cavity of sporopollenin. As can be seen, MgO and magnetic nanoparticles were distributed and anchored over the holes and walls of sporopollenin in the ranges of 277.9, 119.1, 390.6, and 662.5 nm (Kamboh et al. 2021; Ozyilmaz et al. 2018).

The nanostructure of the MSP@MgO adsorbent was studied with TEM microscopy (Fig. 2d). The light substrate and dark spots show the presence of metal oxide-based nanoparticles (Iron oxide/MgO NPs) on the surface, walls, and craters of sporopollenin. Hence, the TEM image verified that the sporopollenin pores and walls are avoided by the agglomeration of metal oxide nanoparticles. The combination of this type of nano/microstructure improved the surface-to-volume ratio of the material, which increased the adsorption sites of the adsorbent.

Spectroscopy techniques

To prove the presence of MgO nanoparticles on the surface/walls of the MSP matrix, EDX elemental analysis was applied. Figure 3a shows the EDX spectrum of MSP@MgO with various sharp and slight signals, which were related to elements of Mg, C, O, Fe, Au (coating source), and Cd/Ca (impurities). Hence, the main element of MSP@MgO nanocomposite was proved by the presence of Mg, Fe, C, and O elements with weight percentages of 30%, 14%, 23%, and 30%, respectively. These results confirm the presence of iron and magnesium oxide nanoparticles over the surface/walls of sporopollenin, which proven the successful formation of nanocomposites.

Surface functional groups of MSP and MSP@MgO were studied with FTIR spectroscopy (Fig. 3b). The

Fig. 2 SEM micrographs of **a** plain sporopollenin, **b** MgO NPs, and **c** MSP@MgO adsorbent with 5 kx magnification. **d** TEM image for MSP@MgO nanocomposite

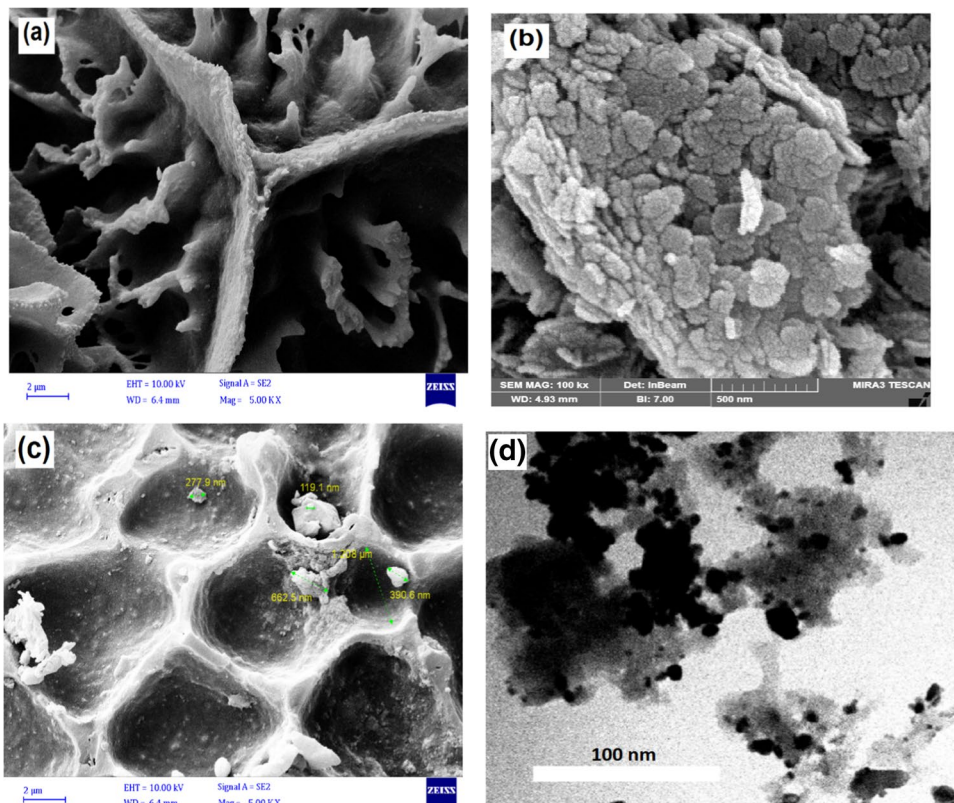
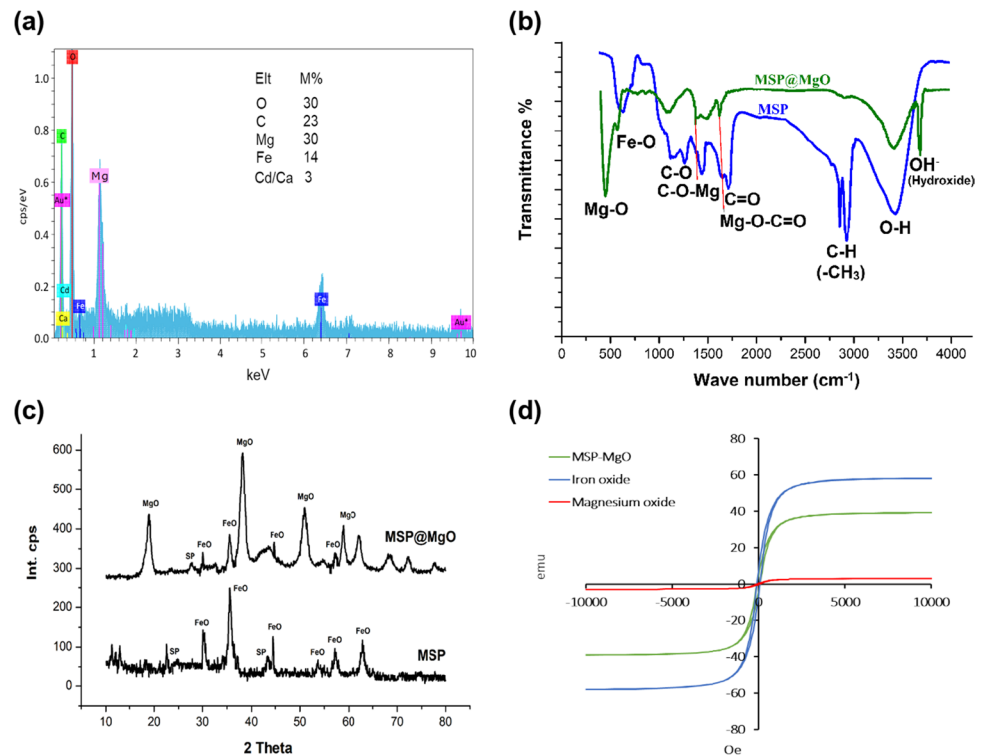


Fig. 3 **a** EDX spectrum and elemental composition. **b** FTIR spectra for MSP and MSP@MgO. **c** XRD pattern for MgO and MSP@MgO. **d** VSM hysteresis loop for plain MNPs, MgO and MSP@MgO



spectra of MSP show various broad/sharp IR bands at 3404 cm^{-1} , 2998 cm^{-1} , 1701 cm^{-1} , 1430 cm^{-1} , 1247 cm^{-1} , 1066 cm^{-1} , and 580 cm^{-1} that indicated vibration stretching of O-H, C-H, C=O, C-C, C-O, C-O-H, and Fe-O, respectively. These functional groups corresponding to sporopollenin and Fe-O performs the presence of magnetic iron oxide on SP (Ahmad et al. 2017; Dyab et al. 2018). After spotting of MgO nanoparticles over the MSP substrate, a new sharp IR band was observed at 590 cm^{-1} , which is corresponding to Mg-O vibration stretching. Since metal oxide (M-O) bands were observed at $450\text{--}600\text{ cm}^{-1}$ (Rajabi et al. 2017). Hence, the appearance/disappearance/of IR bands and decreasing the intensity of some IR bands in final product spectra as compared to plain MSP demonstrated the successful synthesis of MSP@MgO nanocomposite.

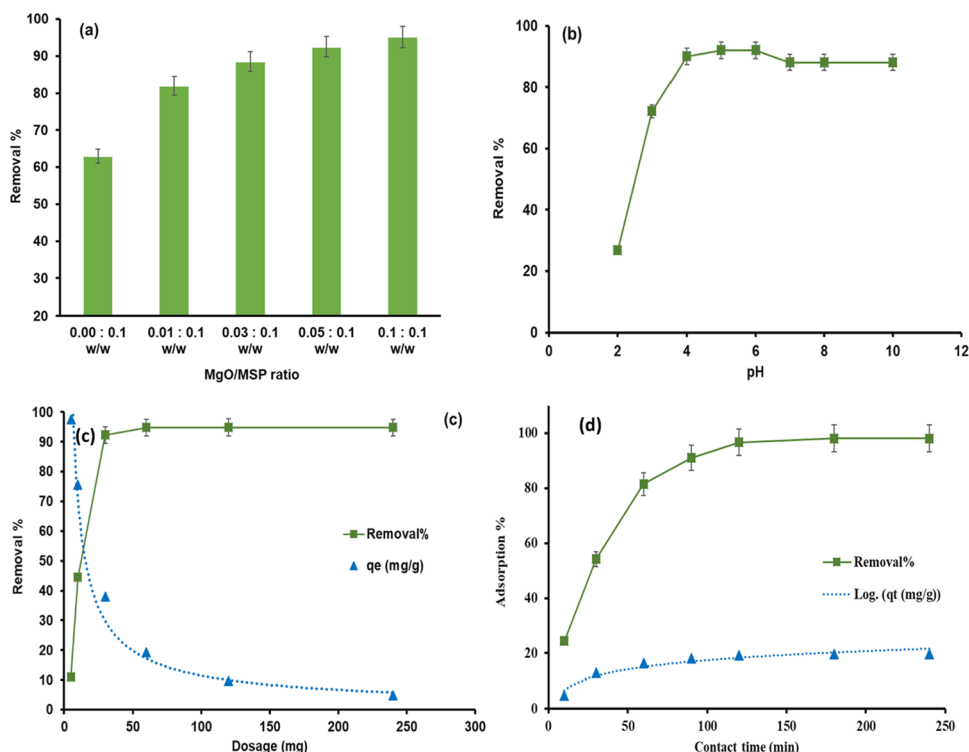
Figure 3c illustrates the XRD pattern of MSP and MSP-MgO nanocomposite which confirmed the successful synthesis and high crystallinity of the adsorbent. In the XRD pattern of MSP, several diffraction peaks were recognized for FeO nanoparticles inside 2θ as 30.15° (220), 35.5° (311), 43.13° (400), 53.49° (422), and 56.99° (511) (Science-poland 2017). Furthermore, SP due to having an amorphous structure, there were no significant peaks in the spectrum; hence, two weak peaks were located at 20° and 42° (Sahin and Hilal 2012). The crystalline structure of nanocomposite was investigated

as well. Although all peaks present in the spectrum were considered for MSP, the strong and sharp peaks at 37.1° , 56.49° , 62.5° attributed to (200), (111), and (220), which is the XRD JCPDS no. 01-075-0447 are assigned the lattice plane of MgO in cubic crystals. Hence, the XRD pattern is associated with MgO nanoparticles in the structure of nanocomposite (El-sayyad et al. 2018).

Vibrating sample magnetometer

The magnetic properties of the adsorbent material play an imperative role in the magnetic adsorption process. Since it helps in the collection of magnetic adsorbents from a large volume of aqueous media with the assistance of an external magnet. Hence, the magnetic properties of MSP@MgO nanocomposite were analyzed with the VSM technique. In this regard, the magnetization saturation hysteresis curve for plain magnesium oxide (MgO NPs), iron oxide, and modified MSP@MgO are shown in Fig. 3d. The VSM depicts a very low magnetic saturation level for MgO (1.1 emu) and high magnetic saturation for iron oxide (58 emu). The saturation magnetization was achieved ~ 32 emu for modified MSP@MgO nanocomposite. The small decrease in magnetic level as compared to iron oxide is probably due to the presence of bulk sporopollenin and MgO NPs. However, the value of 32 emu indicated good magnetic behavior for MSP@MgO adsorbent, which is applicable in the magnetic adsorption process.

Fig. 4 **a** Effect of different ratios of adsorbent, **b** solution's pH on TC removal, **c** removal efficiency ($R\%$) and adsorption capacity (q_e) for TC over different dosages of MSP@MgO. **d** effect of contact time on TC removal efficiency ($R\%$) and adsorption capacity (q_t) at different times. Experimental condition: sample 40 mL, TC 30 mg. L⁻¹, adsorbent 50 mg, pH 5, contact time 120 min



Effective parameter on adsorption

The ratio of adsorbent material

The influence of the different ratios of MgO and its synergistic effect was examined (Fig. 4a). According to the results, with increasing MgO nanoparticles in the structure of the nanocomposite, the increment in the removal percentage can be seen obviously. The best ratio to achieve the highest level of extraction efficiency was at (0.1:0.1) for MgO and MSP. This phenomenon can be associated with the enhancement of the surface-to-volume ratio of nanocomposite and more interaction with tetracycline, resulting in boosting the removal of tetracycline.

Effect of pH

Since the surface of adsorbent and adsorbate can be affected by pH, the impact of different pH on the removal efficiency was determined. The experiment was performed over a wide range of 2 to 10 in the constant condition (30 mg.L⁻¹ concentration of TC). According to Fig. 4b, initially, with increasing pH up to 4, the removal percentage increased sharply, then at a higher pH, the trend kept invariant. These changes were associated with changes in the chemical backbone of TC and MSP@MgO in different conditions. TC has three pKa at 3.3, 7.68, and 9.68, therefore this molecule can be ionized at various pH. Hence, due to the zeta potential value for MSP ~ 3–4 (Kamboh

et al. 2021; Sereshti et al. 2020), in acidic circumstances (pH < 3.3), the amine groups of the TC molecule become protonated and the whole molecule positively charged. On the other hand, under such circumstances, hydroxyl and carboxylic groups in the structure of sporopollenin (MSP@MgO) possess a positive charge in an acidic medium (Kamboh et al. 2021). In this regard, due to the repulsion interactions, the removal efficiency was low. After enhancing pH, the results showed the maximum extraction efficiency due to the neutralization of TC at pH between 3.32 and 7.78. At higher pH (> 7) and alkaline conditions, the MSP@MgO and TC molecules lose their protons and find a negative charge on the surface (Alidadi et al. 2018; Zhang et al. 2015). Hence, pH 5 was selected as optimum for further experiments.

Effect of adsorbent dosage

The study of the impact of different adsorbent doses in the range of (5–240 mg) was carried out as shown in Fig. 4c. In the initial stage, when the adsorbent dosage increased to 30 mg, the removal percentage was increased promptly due to vacant active sites on the surface of MSP@MgO for binding with tetracycline. Gradually, with increasing dosage to above 30 mg, the decline was observed in the trend resulting from the occupation of all active positions; hence, adsorption capacity decreased as well. Eventually, 30 mg was regarded as an optimum adsorbent dosage for further experiments.

Contact time

To obtain equilibrium time and maximum adsorption, the investigation of a different time in the range of 10 to 240 min was performed. As shown in Fig. 4d, by increasing the time from 10 to 180 min, the removal percentage increased dramatically from 24.45 to 98.05%. Thereafter, when the time reached 180 min, equilibrium was obtained and after this time, the trend remained unchanged. Finally, 180 min was considered as an equilibrium time for the adsorption of TC.

Adsorption kinetic

The adsorption kinetic is important for the evaluation of the adsorption process. Then, pseudo-first-order, pseudo-second-order, Elovich, and intraparticle diffusion models were exploited for justifying adsorption efficiency. The selected models can be explained by Eqs. 3, 4, 5 and 6, respectively.

$$\ln(q_e - q_t) = \ln q_e - k_1 t \tag{3}$$

$$\frac{t}{q_t} = \frac{1}{k_2 q_e^2} + \frac{t}{q_e} \tag{4}$$

$$q_t = k_{id} t^{1/2} + C_i \tag{5}$$

$$q_t = \left(\frac{1}{\beta}\right) \ln(\alpha\beta) + \left(\frac{1}{\beta}\right) \ln(t) \tag{6}$$

In these, q_t (mg.g^{-1}) is the concentration of TC adsorbed at time t (min), q_e (mg.g^{-1}) is attributed to the concentration of TC adsorption at equilibrium, K_1 is the pseudo-first-order constant and K_2 is a pseudo-second-order constant. The linear plot (Fig. 5a and b) of pseudo-first-order and pseudo-second-order are obtained based on $\ln(q_e - q_t)$ vs t and t/q_t vs t . In the intraparticle diffusion equation the K_{id} ($\text{mg/g.min}^{1/2}$) is diffusion rate constant, C_i is boundary layer thickness, which is obtained from a linear plot of q_t vs $t^{1/2}$ (Fig. 5c) (Vahidhabanu et al. 2019). Elovich model parameters are including, α (mg/g.min) initial adsorption rate and reflect the adsorption quantity, β (g/mg) is constant and reflects the number of available adsorption (Eldin et al. 2020), which are calculated from q_t vs $\ln(t)$ (Fig. 5d). The values of the parameters are listed in Table 1.

Figures 5 a and b illustrate fitted curves for models, and data show that pseudo-second order possesses a higher coefficient ($R^2 = 0.994$) than pseudo-first-order ($R^2 = 0.804$). It can be concluded that experimental results agreed with pseudo-second-order models, and this model can describe the adsorption process. The high R^2 shows the experimental

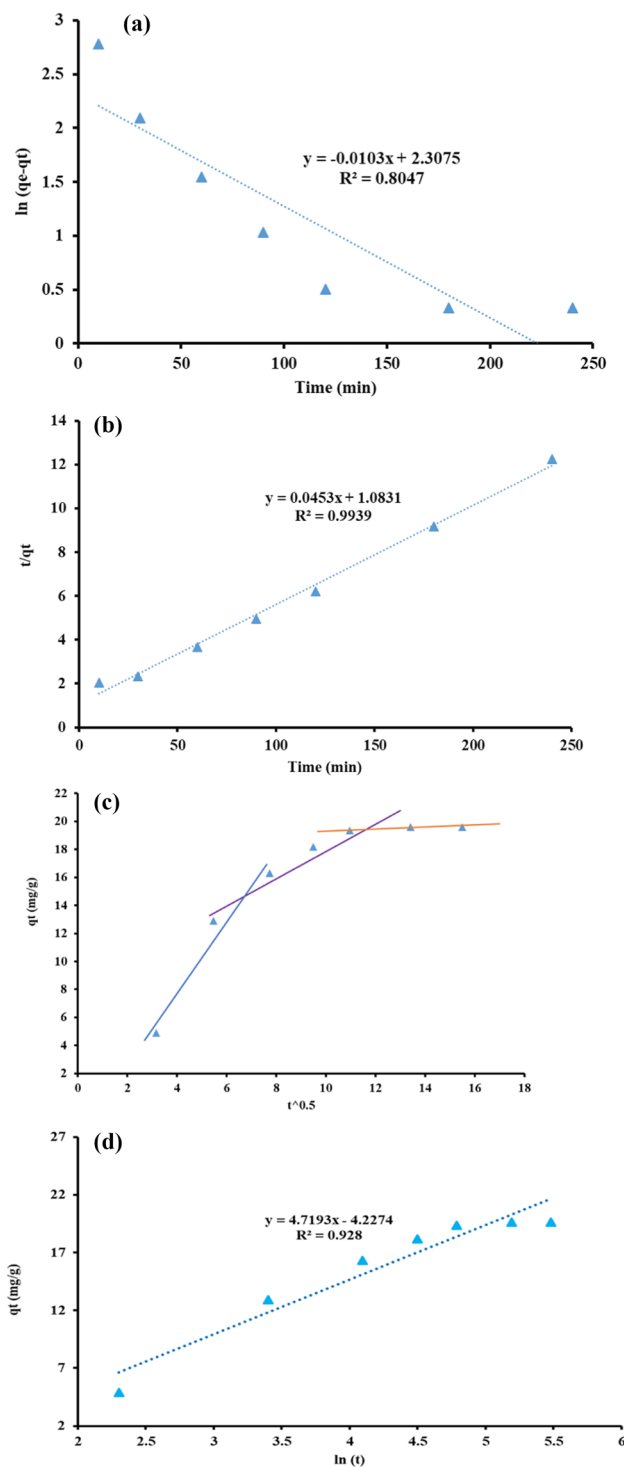


Fig. 5 a pseudo-first-order and b pseudo-second-order, c Elovich and d intraparticle diffusion models

process agreed with the Elovich model and confirmed that the kinetic rate was limited with pseudo second order (Ojedokun and Bello 2017). Intraparticle diffusion provided three-step adsorption rates, due to the presence of sporopollenin pores/walls and MgO nanoparticles.

Table 1 Kinetic parameters for the adsorption of TC on the MSP@MgO

Models	Parameters	TC
pseudo-first- order	R^2	0.804
	k_1 (1/min)	0.014
	q_e (mg.g ⁻¹)	8.53
pseudo-second- order	R^2	0.993
	k_2 (g/mg/min)	0.002
	q_e (mg.g ⁻¹)	22.07
Intraparticle diffusion	K_{id} 1, 2, 3	2.49, 1.18, 0.06
	C_i 1, 2, 3	2.25, 6.72, 18.71
	R^2 , 1, 2, 3	0.951, 0.981, 0.791
Elovich	α	0.89
	β	0.22
	R^2	0.928

Study of adsorption isotherm and thermodynamic

To study the adsorption isotherm, the initial concentration of TC varied from 10 to 200 mg/L as shown in Fig. 6a. At the isotherm process, the equilibrium adsorption capacity increased and the removal efficiency decreased by increasing the TC concentration at room temperature. This trend was due to decreasing the adsorption sites per amount of adsorbate. Moreover, the behavior of adsorption of TC on the MSP@MgO at room temperature was studied using two common isotherm models including Langmuir and Freundlich (Eqs. 7 and 8). Langmuir model assumes a homogeneous monolayer cover of adsorbate on the surface, and the Freundlich model describes a heterogeneous cover of molecules on the surface. The linear form of the Langmuir and Freundlich models is plotted in Fig. 6b and c and their parameters are listed in Table 2. In addition, the linear plots (Fig. 6b and c) and Table 2 are demonstrated that both Langmuir and Freundlich well fitted on experimental data due to the determination of coefficient (R^2) > 0.94. However, the models suggesting the adsorption progress were justified using both models and the adsorption of TC on the surface of nanocomposite was monolayer and multilayer at the homogeneous and heterogeneous surface, respectively.

$$\frac{1}{q_e} = \frac{1}{bC_e q_m} + \frac{1}{q_m} \quad (7)$$

$$\ln q_e = K_F \times \frac{1}{n} \ln(C_e) \quad (8)$$

where C_e (mg/g) is equilibrium concentration, q_m (mg/g) is the maximum adsorption capacity of Langmuir, b (L.mg)

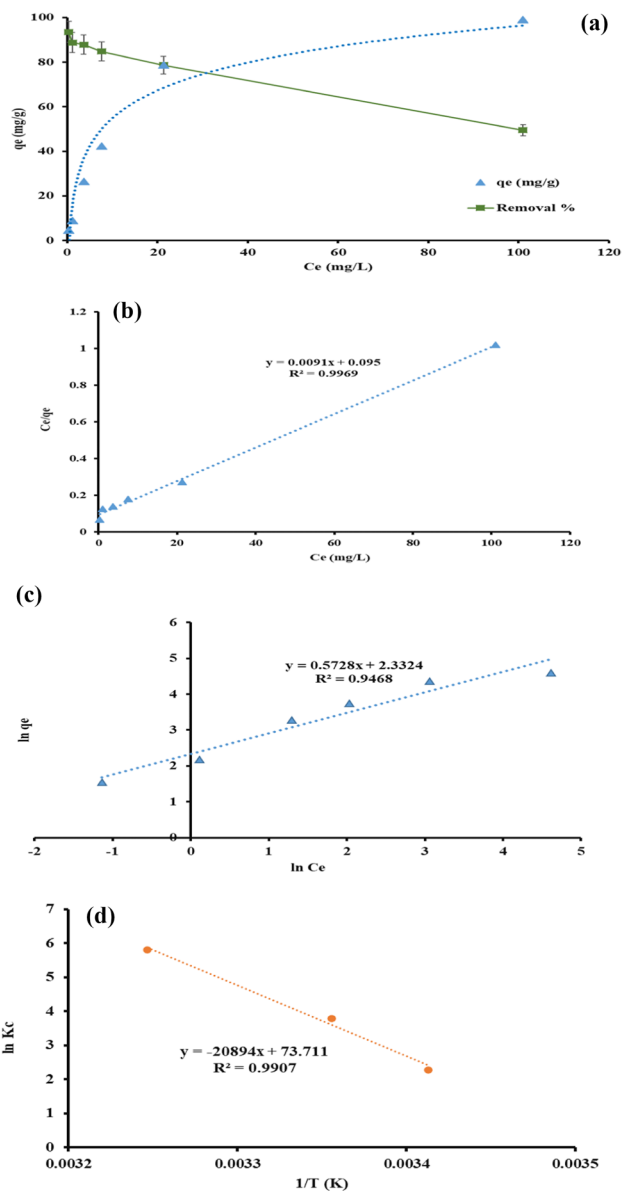


Fig. 6 a effect of initial concentration, a linear plot of **b** Langmuir and **c** Freundlich isotherm models. **d** thermodynamic linear plot at different temperatures

is the constant of adsorption energy, K_F [(mg/g) (L/mg)^{1/n}] is Freundlich constant and n is related to the heterogeneous factor.

$$\Delta G^\circ = -RT \ln K_D \quad (9)$$

$$\ln K_D = -\frac{\Delta H^\circ}{RT} + \ln \frac{\Delta S^\circ}{R} \quad (10)$$

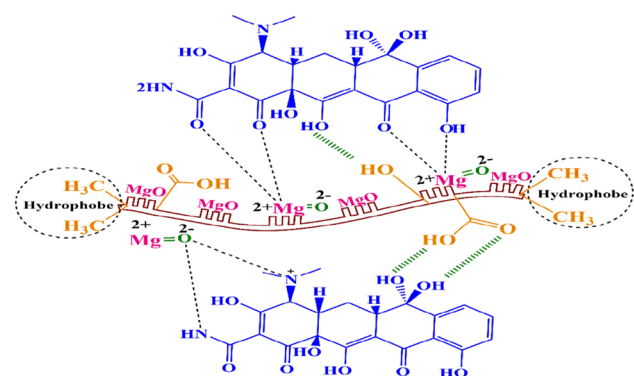
$$K_D = \frac{1000 q_e}{C_e} \quad (11)$$

Table 2 Comparison of the adsorption process for Langmuir and Freundlich isotherm models

Analyte	Langmuir model			Freundlich model		
	q_m (mg.g ⁻¹)	K_L (L.mg ⁻¹)	R ²	1/n (mg.g ⁻¹)	K_F (mg.L ⁻¹) ^{-1/n}	R ²
TC	109.890	0.0957	0.997	1.748	8.775	0.946

Table 3 Thermodynamic parameters for the adsorption process at different temperatures

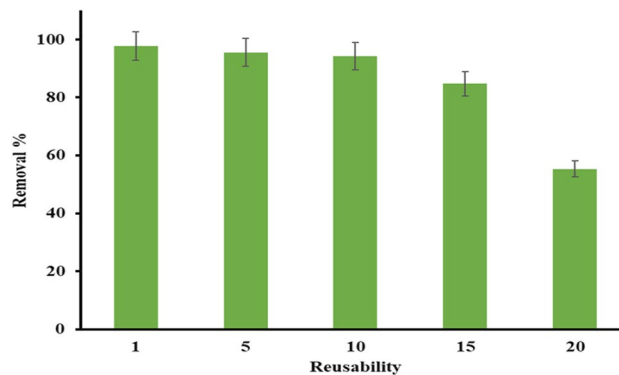
Analyte	T(K)	Q _e (mg/g)	ΔG(KJ/mol)	ΔH(KJ/mol.K)	ΔS(KJ/mol.K)
TC	293	45.33	-5.53	17.36	0.599
	298	48.89	-9.39		
	308	49.85	-14.86		

**Fig. 7** The mechanism of adsorption of TC on the MSP@MgO

In these equations, ΔG is Gibbs free energy change, ΔS is entropy and ΔH is enthalpy change and K_D is a dimensionless quantity of thermodynamic constant.

Temperature and thermodynamic study

In a further study, the influence of the ambient temperature (isotherm) and varied temperature on the adsorption process was investigated. The adsorption process was investigated at different temperatures (293, 298, and 308 K), which is validated with thermodynamic models (Eqs. 9–11). The linear plot of the thermodynamic ($\ln K_c$ vs $1/T$) is shown in Fig. 6d. The thermodynamic parameters were calculated and listed in Table 4. Hence, by increasing temperature, the adsorption capacity reached 45.33 to 49.85 mg.g⁻¹, which performs the high temperature and is favorable for the adsorption progress. Furthermore, according to Table 3, the adsorption phenomenon was endothermic due to the positive value of enthalpy ($\Delta H > 0$). Also, the adsorption process is randomness ($\Delta S > 0$) and spontaneous ($\Delta G < 0$). However, the mechanism of TC adsorption over MSP@MgO is

**Fig. 8** Recyclability of MSP@MgO for the removal of TC

following the physisorption mechanism, due to the values of ΔG , which are less than -20 KJ/mol.

Adsorption mechanism

The suggested mechanism of adsorption of TC on the surface of MSP@MgO is depicted in Fig. 7. There are some dominant interactions including electrostatic and H-bonding which lead to adsorption and elimination of TC from the solution. TC molecule conformation has three active sites such as -NH, -OH, and -O that can bind with other active sites. Since sporopollenin has various functional groups such as hydroxyl and carboxylic groups, on its backbone it can contribute to functional groups in the TC structure. -NH and -OH are involved with hydrogen binding with -OH and -COOH in the structure of sporopollenin. Furthermore, the attraction force that occurred between $Mg^{2+} \dots O^{2-}$ could assist in the removal of TC (Moussavi et al. 2018; Yue et al. 2019). These interactions were the most probable interactions that could enhance the removal efficiency of TC by MSP@MgO.

Reusability or desorption study

From an economic standpoint, the assessment regeneration of adsorbent is required, which is examined using the desorption process. For this purpose, the experiment was carried out after adding 100 mg adsorbent to the solution which contained 30 mg.L⁻¹ TC at pH 5. Then, the solution was mixed for 120 min to achieve equilibrium. After

Table 4 Comparison of current study with other published studies

Adsorbent	Adsorbate	pH	Time (min)	%R	Q (mg.g ⁻¹)	Ref.
MSP@MgO	TC	5	120	> 91	109	This study
Cu-Alginate	TC	3	60	90	53.26	(Zhang et al. 2019)
IL-CNTs	TC	4	12	99	40	(Chen et al. 2021)
ZIF-8-MGO	TC	5	10	99	382	(Wang et al. 2020)
Zr-MOF	TC	5	40	> 90	145	(Xia et al. 2021)
M-Rice strew	TC	4	60	69	93.5	(Dai et al. 2020)

reaching equilibrium, the adsorbent was separated with the assistance of a magnet, then the adsorbed TCs were desorbed with methanol (3 mL for 10 min). This experiment was accomplished for 20 consecutive adsorption-desorption cycles and the results can be seen in Fig. 8. The results demonstrated that after 15 cycles, the removal efficiency was 84.72%, which had an acceptable value (Fig. 8). These results confirmed substantial reusability after 15 times that can be applied as a cost-effective adsorbent for the elimination of TC.

Comparison with the similar studies

In Table 4, the magnetic solid technique based on MSP@MgO nanocomposite is compared with the previously published studies. The mentioned adsorbents were used for the removal/adsorption of tetracyclines from water samples. It showed that the MSP@MgO had a high efficiency (> 91%) for TC as compared Cu-alginate and M-rice. While the current adsorbent showed a lower sorption capacity (109 mg.g⁻¹) as compared to the Zr-MOF (145 mg.g⁻¹) and ZIF-8-MGO (382 mg.g⁻¹), this was due to the high porosity of the MOF-based structure and strong interactions between TCs and the proposed adsorbents.

Conclusions

The present work offered a novel adsorbent that had acceptable results for the elimination of TC from aqueous solutions. The electrostatic interactions and H-bonding were the driving force for the adsorption of TC. Since pH exerted a significant influence on the structure of TC, the impact of this parameter was investigated, and the findings confirmed that pH 5 was optimum for the experiment. The isotherm models for the determination of the mechanism of the process were carried out, and the progress was fitted completely with the Langmuir model. The kinetics of the experiment was studied, and the data was followed by pseudo-second-order. Also, the data derived from thermodynamic parameters at different temperatures approved that the adsorption process was endothermic and spontaneous. Eventually, this work

can give insight into developing a novel adsorbent that is eco-friendly, economical, and has the potential for the removal of antibiotics from aqueous solutions.

Acknowledgements The authors are thankful to the Deanship of Scientific Research at Najran University for funding this work, under the Research Priorities and Najran Research funding program grant code (NU/NRP/SERC/12/41). This research was also financially supported by Prince of Songkla University and Ministry of Higher Education, Science, Research and Innovation under the Reinventing University Project (Grant Number REV65017).

Author contribution JSA investigated the samples and prepared the original draft of the manuscript. Material preparation, data collection, analysis, and supervision were performed by KKY. AG and IHA, investigated and interpreted XRD, FTIR, and PSA results. SR, and MSOA critically evaluated the manuscript. A.M. analyzed and interpreted FESEM micrographs and revised the manuscript. BHJ analyzed and interpreted TEM micrographs. SC prepared the original draft of the manuscript and supervised it. All authors read and approved the final manuscript.

Data availability Data sharing is not applicable to this article as no datasets were generated or analyzed during the current study.

Declarations

Ethical approval Not applicable.

Consent to participate Not applicable.

Consent for publication Not applicable.

Competing interests The authors declare no competing interests.

References

- Ageitos JM, Robla S, Valverde-Fraga L, Garcia-Fuentes M, Csaba N (2021) Purification of hollow sporopollenin microcapsules from sunflower and chamomile pollen grains. *Polymers* 13. <https://doi.org/10.3390/polym13132094>
- Ahmad NF, Kamboh MA, Nodeh HR, Halim SNBA, Mohamad S (2017) Synthesis of piperazine functionalized magnetic sporopollenin: a new organic-inorganic hybrid material for the removal of lead(II) and arsenic(III) from aqueous solution. *Environ Sci Pollut Res* 24. <https://doi.org/10.1007/s11356-017-9820-9>
- Ahmed MJ (2017) Adsorption of quinolone, tetracycline, and penicillin antibiotics from aqueous solution using activated carbons:

- review. *Environ Toxicol Pharmacol* 50:1–10. <https://doi.org/10.1016/j.etap.2017.01.004>
- Alidadi H, Dolatabadi M, Davoudi M, Barjasteh-Askari F, Jamali-Behnam F, Hosseinzadeh A (2018) Enhanced removal of tetracycline using modified sawdust: optimization, isotherm, kinetics, and regeneration studies. *Process Saf Environ Prot* 117:51–60. <https://doi.org/10.1016/j.psep.2018.04.007>
- Alvand ZM, Rajabi HR, Mirzaei A, Masoumiasl A, Sadatfaraji H (2019) Rapid and green synthesis of cadmium telluride quantum dots with low toxicity based on a plant-mediated approach after microwave and ultrasonic assisted extraction: synthesis, characterization, biological potentials and comparison study. *Mater Sci Eng C* 98:535–544
- Cai W, Weng X, Chen Z (2019) Highly efficient removal of antibiotic rifampicin from aqueous solution using green synthesis of recyclable nano-Fe₃O₄. *Environ Pollut* 247:839–846
- Chaturvedi P, Shukla P, Giri BS, Chowdhary P, Chandra R, Gupta P, Pandey A (2021) Prevalence and hazardous impact of pharmaceutical and personal care products and antibiotics in environment: a review on emerging contaminants. *Environ Res* 194:110664
- Chen C, Feng X, Yao S (2021) Ionic liquid-multi walled carbon nanotubes composite tablet for continuous adsorption of tetracyclines and heavy metals. *J Clean Prod* 286:124937
- Dai J, Meng X, Zhang Y, Huang Y (2020) Effects of modification and magnetization of rice straw derived biochar on adsorption of tetracycline from water. *Bioresour Technol* 311:123455
- dos Santos AJ, Kronka MS, Fortunato GV, Lanza MRV (2021) Recent advances in electrochemical water technologies for the treatment of antibiotics: a short review. *Curr Opin Electrochem* 26:100674. <https://doi.org/10.1016/j.coelec.2020.100674>
- Du C, Zhang Z, Yu G, Wu H, Chen H, Zhou L, Zhang Y, Su Y, Tan S, Yang L (2021) A review of metal organic framework (MOFs)-based materials for antibiotics removal via adsorption and photocatalysis. *Chemosphere* 272:129501
- Dyab AKF, Mohamed MA, Meligi NM, Mohamed SK (2018) Encapsulation of erythromycin and bacitracin antibiotics into natural sporopollenin microcapsules: antibacterial, cytotoxicity, in vitro and in vivo release studies for enhanced bioavailability. *RSC Adv* 8:33432–33444. <https://doi.org/10.1039/C8RA05499A>
- El-sayyad GS, Mosallam FM, El-batal AI (2018) One-pot green synthesis of magnesium oxide nanoparticles using *Penicillium chrysogenum* melanin pigment and gamma rays with antimicrobial activity against multidrug-resistant microbes. *Adv Powder Technol*. <https://doi.org/10.1016/j.apt.2018.07.009>
- Eldin MSM, Aggour YA, Elaassar MR, Beghet GE, Atta RR (2020) Development of nano-crosslinked polyacrylonitrile ions exchanger particles for dye removal: kinetic, isotherm, and thermodynamic studies. *Desalin Water Treat* 175:24911
- Kabir MM, Alam F, Akter MM, Gilroyed BH, Didar-ul-Alam M, Tijing L, Shon HK (2022) Highly effective water hyacinth (*Eichhornia crassipes*) waste-based functionalized sustainable green adsorbents for antibiotic remediation from wastewater. *Chemosphere* 304:135293
- Kamboh MA, Arain SS, Jatoti AH, Sherino B, Algarni TS, Al-onazi WA, Al-Mohaimeed AM, Rezaia S (2021) Green sporopollenin supported cyanocalixarene based magnetic adsorbent for pesticides removal from water: kinetic and equilibrium studies. *Environ Res* 25:111588
- Koch N, Islam NF, Sonowal S, Prasad R, Sarma H (2021) Environmental antibiotics and resistance genes as emerging contaminants: methods of detection and bioremediation. *Curr Res Microb Sci* 2:100027
- Krasucka P, Pan B, Ok YS, Mohan D, Sarkar B, Oleszczuk P (2021) Engineered biochar—a sustainable solution for the removal of antibiotics from water. *Chem Eng J* 405:126926
- Li M, Liu Y, Yang C, Liu S, Tan X, He Y, Liu N, Zhou L, Cai X, Wen J (2020) Effects of heteroaggregation with metal oxides and clays on tetracycline adsorption by graphene oxide. *Sci Total Environ* 719:137283. <https://doi.org/10.1016/j.scitotenv.2020.137283>
- Liao Q, Rong H, Zhao M, Luo H, Chu Z, Wang R (2021) Interaction between tetracycline and microorganisms during wastewater treatment: a review. *Sci Total Environ* 757:143981. <https://doi.org/10.1016/j.scitotenv.2020.143981>
- Maged A, Iqbal J, Kharbish S, Ismael IS, Bhatnagar A (2020) Tuning tetracycline removal from aqueous solution onto activated 2: 1 layered clay mineral: characterization, sorption and mechanistic studies. *J Hazard Mater* 384:121320
- Moussavi G, Mashayekh-salehi A, Yaghmaeian K, Mohseni-bandpei A (2018) The catalytic destruction of antibiotic tetracycline by sulfur-doped manganese oxide (S e MgO) nanoparticles. *J Environ Manage* 210:131–138. <https://doi.org/10.1016/j.jenvman.2018.01.004>
- Muriuki CW, Home PG, Raude JM, Ngumba EK, Munala GK, Kairigo PK, Gachanja AN, Tuhkanen TA (2020) Occurrence, distribution, and risk assessment of pharmaceuticals in wastewater and open surface drains of peri-urban areas: case study of Juja town, Kenya. *Environ Pollut* 267:115503
- Ngigi AN, Magu MM, Muendo BM (2020) Occurrence of antibiotics residues in hospital wastewater, wastewater treatment plant, and in surface water in Nairobi County, Kenya. *Environ Monit Assess* 192:1–16
- Ojedokun AT, Bello OS (2017) Kinetic modeling of liquid-phase adsorption of Congo red dye using guava leaf-based activated carbon. *Appl Water Sci* 7:1965–1977
- Ozyilmaz E, Etc K, Sezgin M (2018) *Candida rugosa* lipase encapsulated with magnetic sporopollenin: design and enantioselective hydrolysis of racemic arylpropanoic acid esters. *Prep Biochem Biotechnol* 48:887–897. <https://doi.org/10.1080/10826068.2018.1514516>
- Priya SS, Radha KV (2017) A review on the adsorption studies of tetracycline onto various types of adsorbents. *Chem Eng Commun* 204:821–839. <https://doi.org/10.1080/00986445.2015.1065820>
- Rajabi HR, Naghiha R, Kheirizadeh M, Sadatfaraji H, Mirzaei A, Alvand ZM (2017) Microwave assisted extraction as an efficient approach for biosynthesis of zinc oxide nanoparticles: synthesis, characterization, and biological properties. *Mater Sci Eng C* 78:1109–1118
- Saadati F, Keramati N, Ghazi MM (2016) Influence of parameters on the photocatalytic degradation of tetracycline in wastewater: a review. *Crit Rev Environ Sci Technol* 46:757–782. <https://doi.org/10.1080/10643389.2016.1159093>
- Sahin M, Hilal I (2012) Synthesis and characterization of sporopollenin-supported schiff bases and ruthenium (III) Sorption Studies 1279–1286. <https://doi.org/10.1007/s10904-012-9739-z>
- Science-poland M (2017) Solvothermal synthesis and characterization of magnetic Fe₃O₄ nanoparticle by different sodium salt sources. <https://doi.org/10.1515/msp-2017-0004>
- Sereshti H, Toloutehrani A, Nodeh HR (2020) Determination of cholecalciferol (vitamin D3) in bovine milk by dispersive micro-solid phase extraction based on the magnetic three-dimensional graphene-sporopollenin sorbent. *J Chromatogr B* 1136:121907
- Shao S, Wu X (2020) Microbial degradation of tetracycline in the aquatic environment: a review. *Crit Rev Biotechnol* 40:1010–1018. <https://doi.org/10.1080/07388551.2020.1805585>
- Vahidhabanu S, Adeogun AI, Babu BR (2019) Biopolymer-grafted, magnetically tuned halloysite nanotubes as efficient and recyclable spongelike adsorbents for anionic azo dye removal. *ACS omega* 4:2425–2436
- Wang X, Yin R, Zeng L, Zhu M (2019) A review of graphene-based nanomaterials for removal of antibiotics from aqueous environments. *Environ Pollut* 253:100–110

- Wang Z, Chen X, Meng Z, Zhao M, Zhan H, Liu W (2020) A water resistance magnetic graphene-anchored zeolitic imidazolate framework for efficient adsorption and removal of residual tetracyclines in wastewater. *Water Sci Technol* 81:2322–2336
- Xia J, Gao Y, Yu G (2021) Tetracycline removal from aqueous solution using zirconium-based metal-organic frameworks (Zr-MOFs) with different pore size and topology: Adsorption isotherm, kinetic and mechanism studies. *J Colloid Interface Sci* 590:495–505
- Xu L, Zhang H, Xiong P, Zhu Q, Liao C, Jiang G (2021) Occurrence, fate, and risk assessment of typical tetracycline antibiotics in the aquatic environment: a review. *Sci Total Environ* 753:141975
- Yaacob SFFS, Jamil RZR, Suah FBM (2022) Sporopollenin based materials as a versatile choice for the detoxification of environmental pollutants—a review. *Int J Biol Macromol* 207:990–1004
- Yue Y, Peng Z, Wang W, Cai Y, Tan F, Wang X, Qiao X (2019) Facile preparation of MgO-loaded SiO₂ nanocomposites for tetracycline removal from aqueous solution. *Powder Technol.* <https://doi.org/10.1016/j.powtec.2019.02.034>
- Zainab SM, Junaid M, Xu N, Malik RN (2020) Antibiotics and antibiotic resistant genes (ARGs) in groundwater: a global review on dissemination, sources, interactions, environmental and human health risks. *Water Res* 187:116455
- Zhang D, Yin J, Zhao J, Zhu H, Wang C (2015) Adsorption and removal of tetracycline from water by petroleum coke-derived highly porous activated carbon. *J Environ Chem Eng* 3:1504–1512
- Zhang X, Lin X, He Y, Chen Y, Luo X, Shang R (2019) Study on adsorption of tetracycline by Cu-immobilized alginate adsorbent from water environment. *Int J Biol Macromol* 124:418–428

Publisher's note Springer Nature remains neutral with regard to jurisdictional claims in published maps and institutional affiliations.

Springer Nature or its licensor (e.g. a society or other partner) holds exclusive rights to this article under a publishing agreement with the author(s) or other rightsholder(s); author self-archiving of the accepted manuscript version of this article is solely governed by the terms of such publishing agreement and applicable law.